Supporting Information

Gelation of Electron Transport Layer to Improve the Thermal Stability of Efficient Perovskite Solar Cells

Xin Wang, Jingyao Feng, Zaixin Zhang, Jiaojiao Xing, Wenqin Li, Yongjie Cui, Zihua Wu, Wei Yu, Lifei Chen*

Affiliations:

X. Wang, J. Feng, Z. Zhang, J. Xing, W. Li, Y. Cui, Prof. Z. Wu, Prof. W. Yu, Prof. L. Chen*

School of Energy and Materials, Shanghai Key Laboratory of Engineering Materials Application and Evaluation, Shanghai Thermophysical Properties Big Data Professional Technical Service Platform, Shanghai Engineering Research Center of Advanced Thermal Functional Materials,

Shanghai Polytechnic University,

Shanghai 201209, China

E-mail: lfchen@sspu.edu.cn

Supplementary figures.

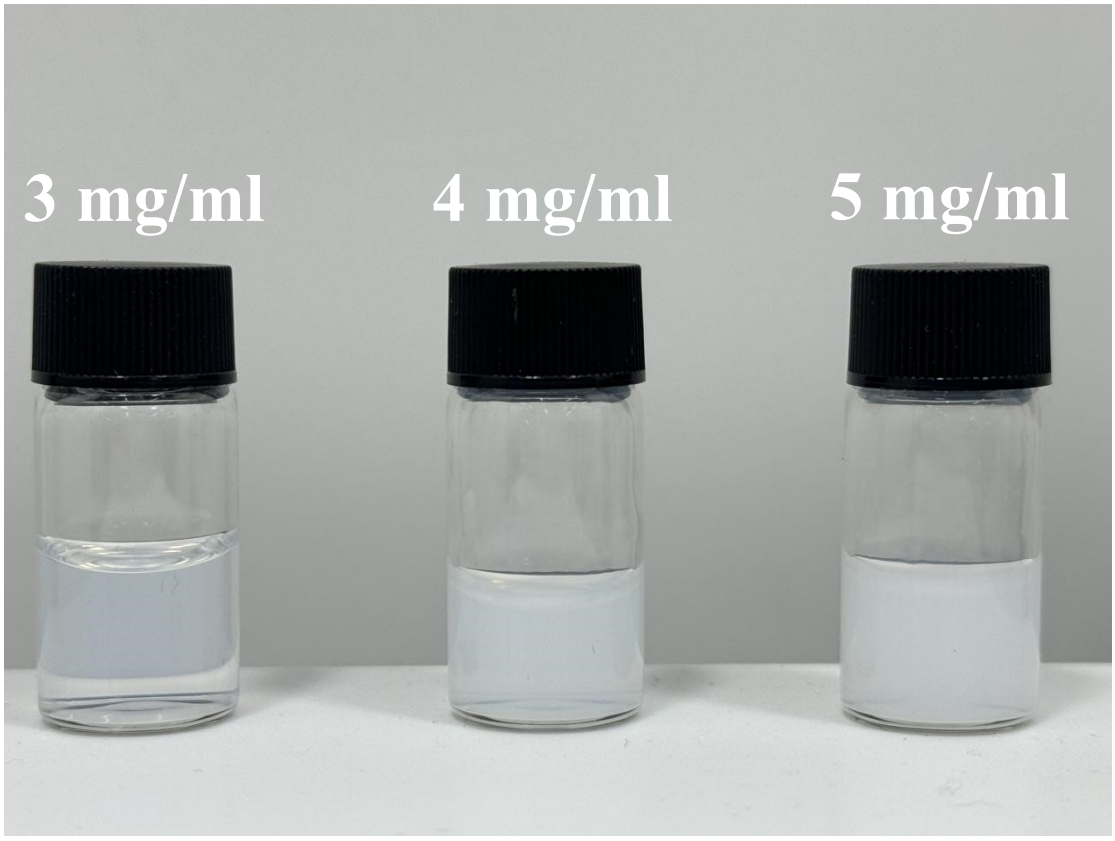

Figure S1. Digital images of SnO_2 colloids with different concentrations of AMO.

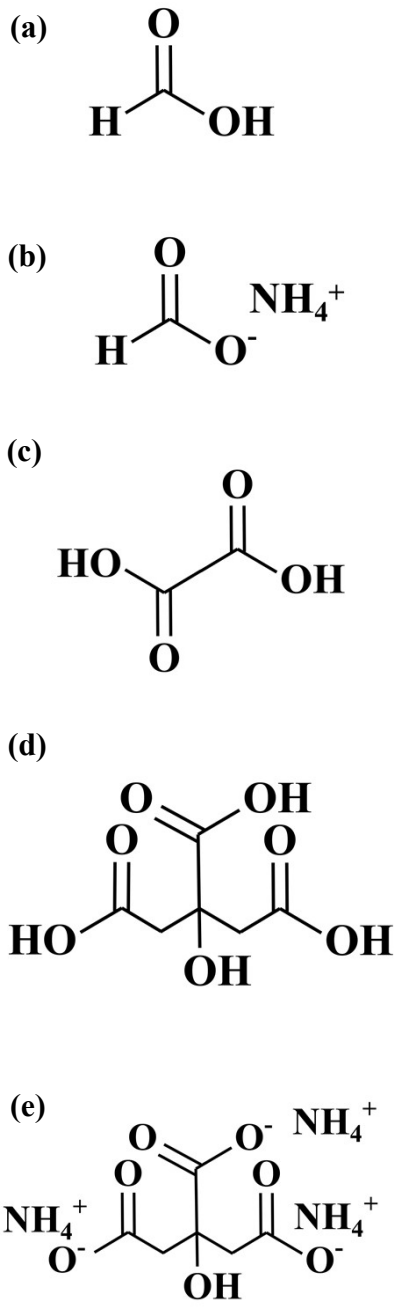

Figure S2. The molecule structure of (a) formic acid, (b) ammonium formate, (c) oxalic acid, (d) citric acid, and (e) ammonium citrate.

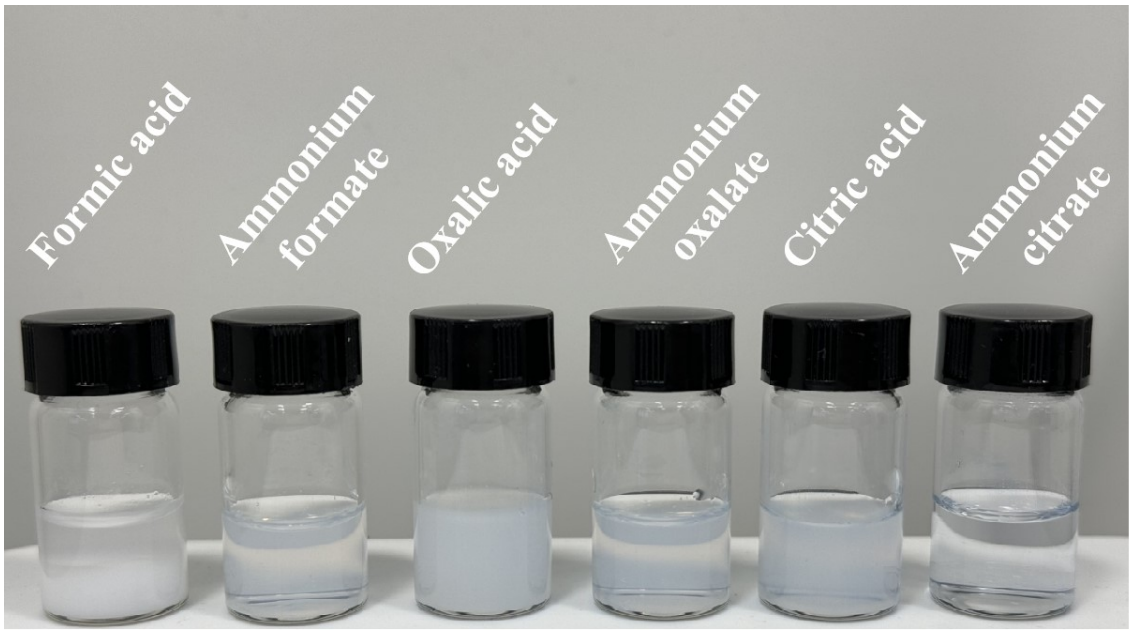

Figure S3. Digital images of gel-like solution of tin oxide with different additives.

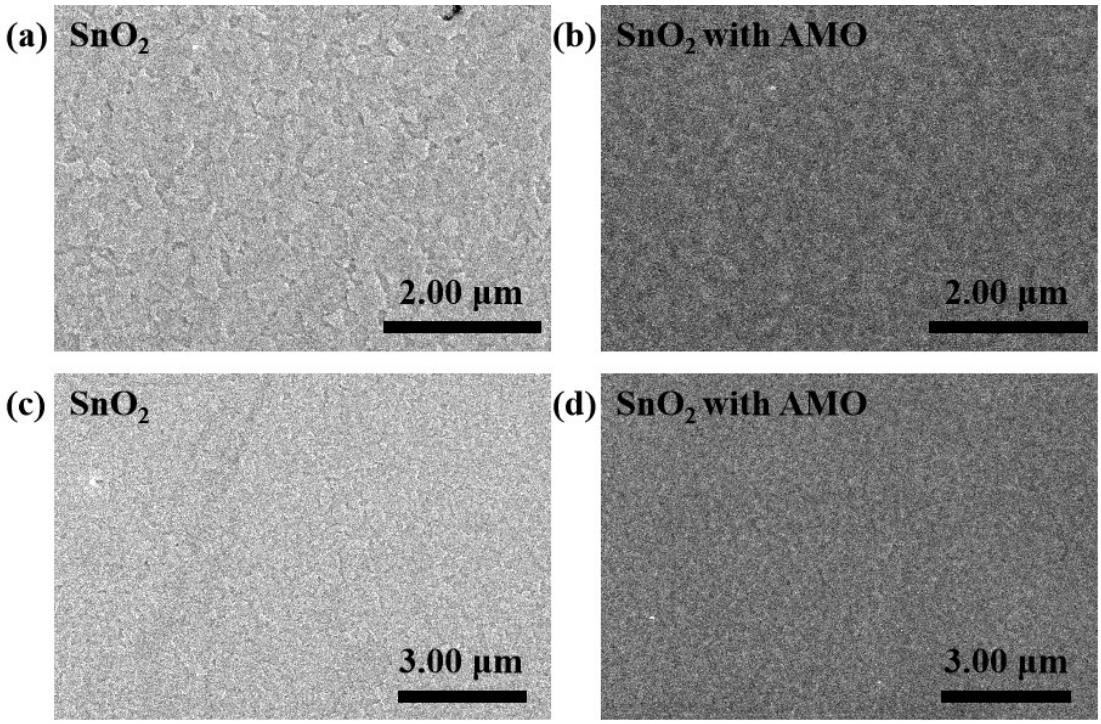

Figure S4. Scanning electron microscopy (SEM) images at different magnifications of SnO_2 and SnO_2 with AMO. (a) and (b) SEM images at 20,000x; (c) and (d) SEM images at 10,000x.

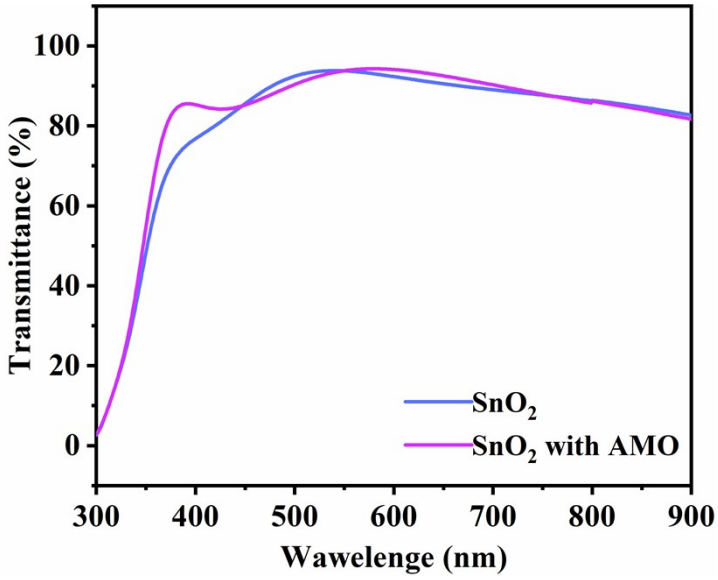

Figure S5. Transmittance spectra of SnO_2 and SnO_2 with AMO films spin-coated on the ITO substrates.

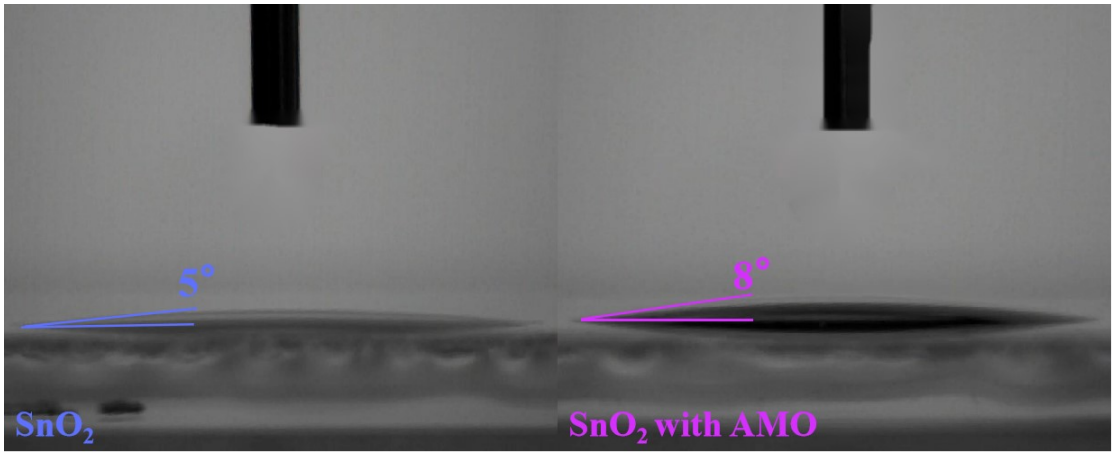

Figure S6. Water droplet contact angles on surfaces of (a) SnO_2 and (b) SnO_2 with AMO films.

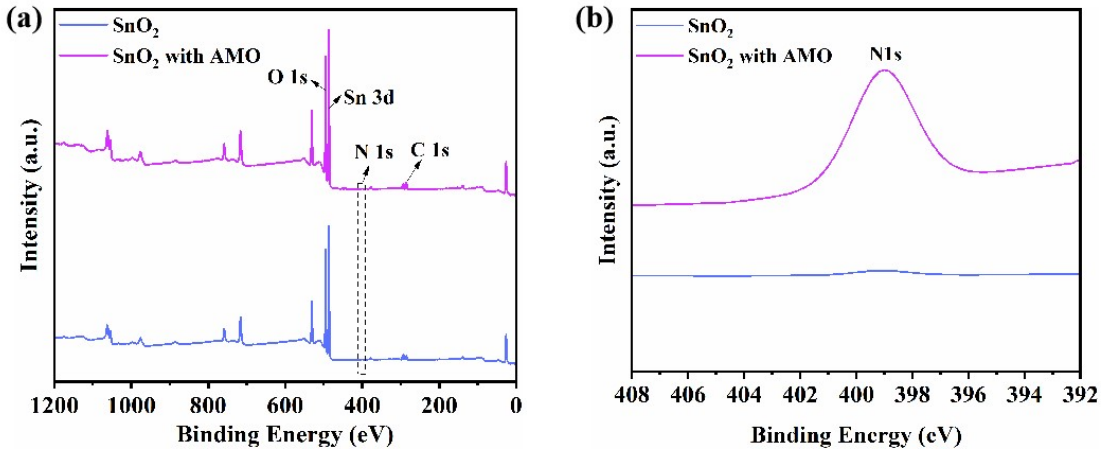

Figure S7. (a) XPS full-spectrum image of SnO_2 and SnO_2 with AMO films spin-coated on the ITO substrates. (b) N1s X-ray photoelectron spectroscopy (XPS) spectra of SnO_2 and SnO_2 with AMO.

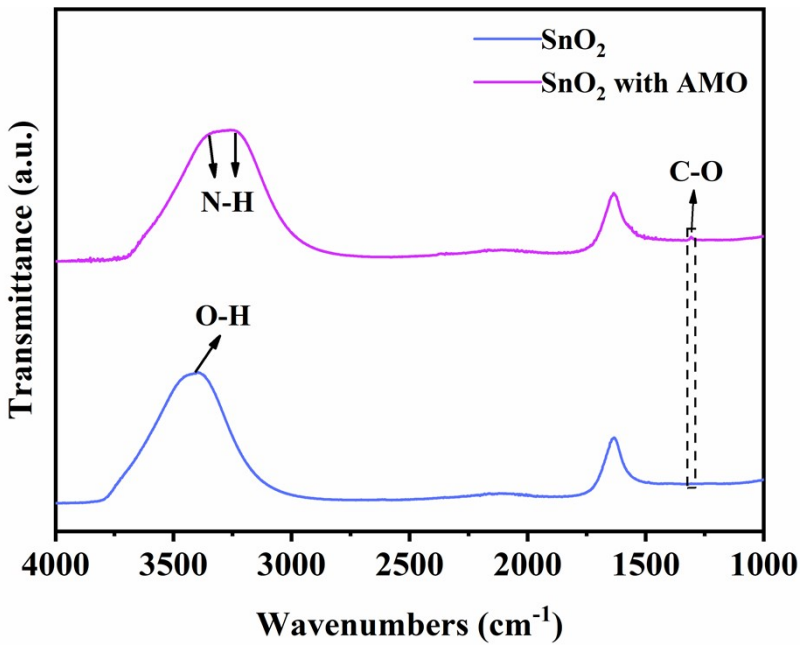

Figure S8. FTIR spectrum of SnO_2 and SnO_2 with AMO films spin-coated on the ITO substrates.

Table S1. Fitted results of TRPL curves of the perovskite films deposited on control and modified SnO_2 films.

Samples	τ_1 (ns)	A_1 (%)	τ_2 (ns)	A_2 (%)	τ_{ave} (ns)
SnO_2	130.8	49.2	347.9	50.8	289.9
SnO_2 with AMO	96.4	49.8	236.1	50.2	195.7

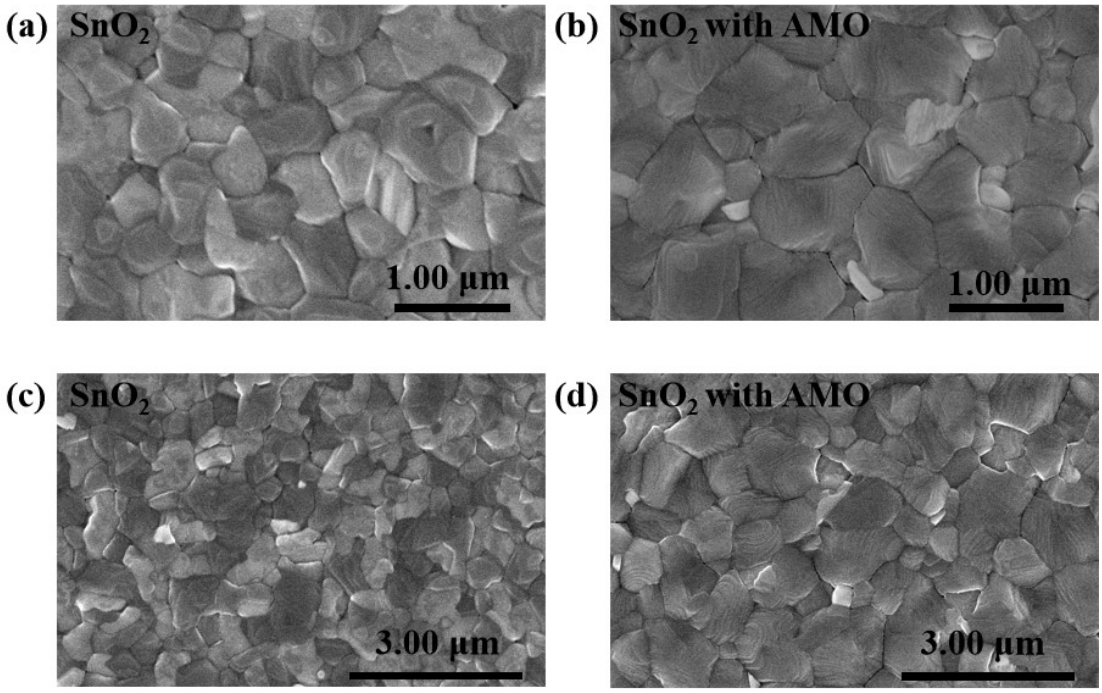

Figure S9. Top-view SEM images of the perovskite films on ETL of SnO_2 and SnO_2 with AMO. (a) and (b) SEM images at 30,000x; (c) and (d) SEM images at 15,000x.

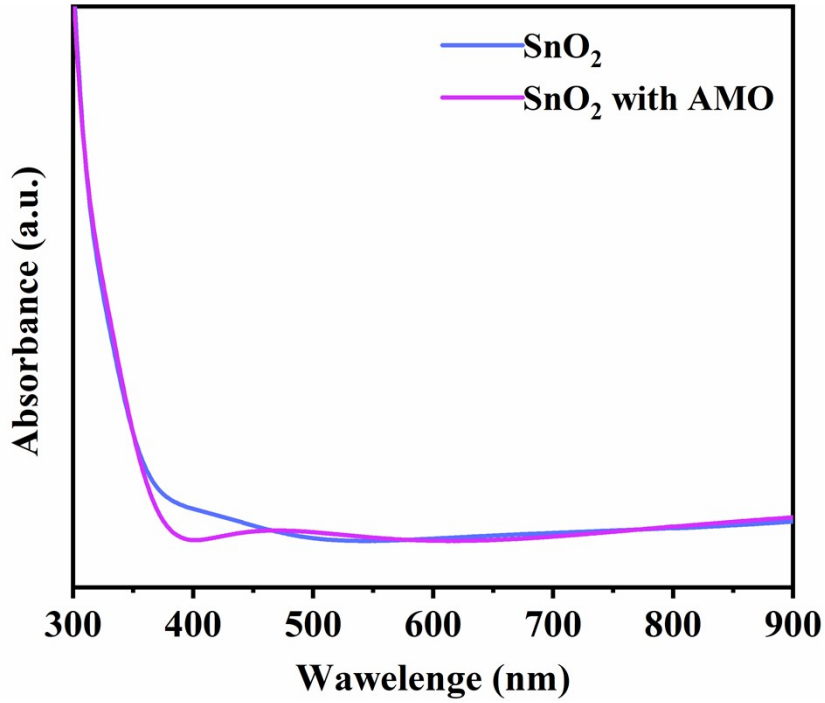

Figure S10. UV-Vis absorption spectra SnO_2 and AMO-SnO_2 films spin-coated on the ITO substrates.

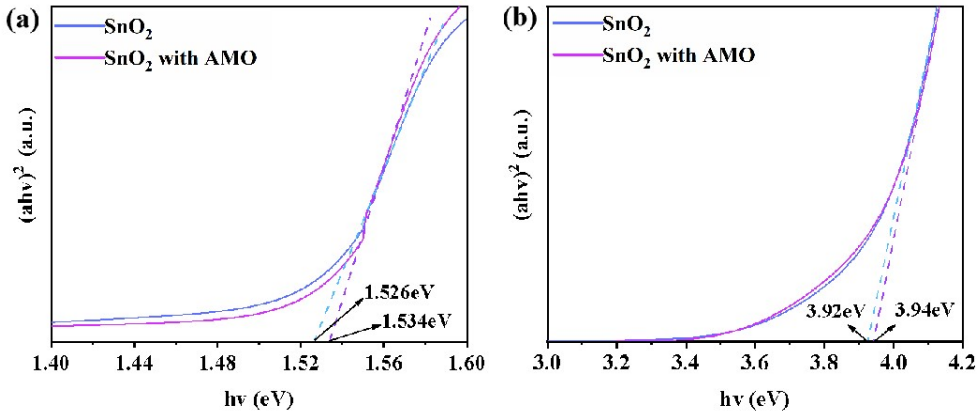

Figure S11. The bandgap of SnO_2 and AMO-SnO_2 for (a) perovskite and (b) ETL.

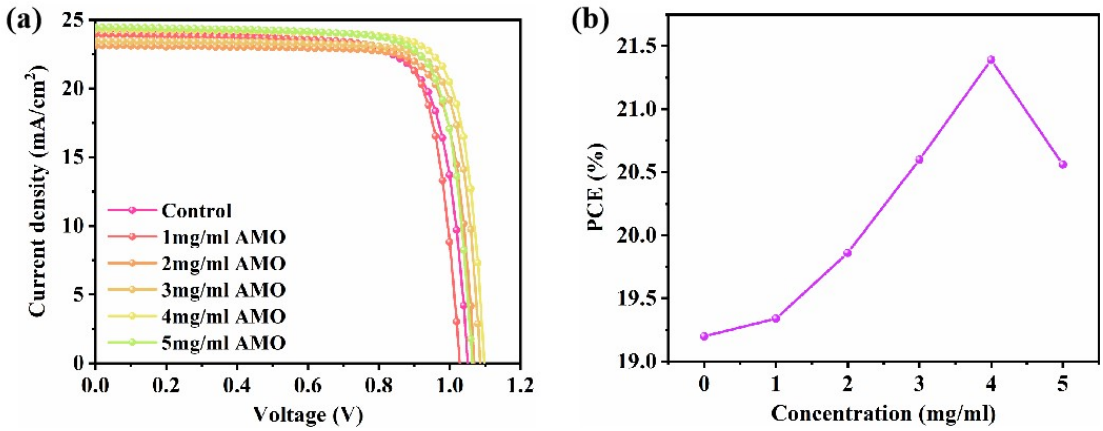

Figure S12. (a) Photovoltaic performance and J-V measurements of devices by different concentrations of ammonium oxalate, and (b) efficiency comparison diagram.

Table S2. Specific photovoltaic parameters of the devices with different concentrations of ammonium oxalate.

Samples	V_{oc} (V)	J_{sc} (mA/cm^2)	FF (%)	PCE (%)
Control	1.05	24.27	75.25	19.20
1mg/ml AMO	1.03	23.94	78.55	19.34
2mg/ml AMO	1.07	23.11	80.30	19.86
3mg/ml AMO	1.09	23.47	80.82	20.60
4mg/ml AMO	1.10	24.31	80.16	21.39
5mg/ml AMO	1.07	24.46	78.95	20.56

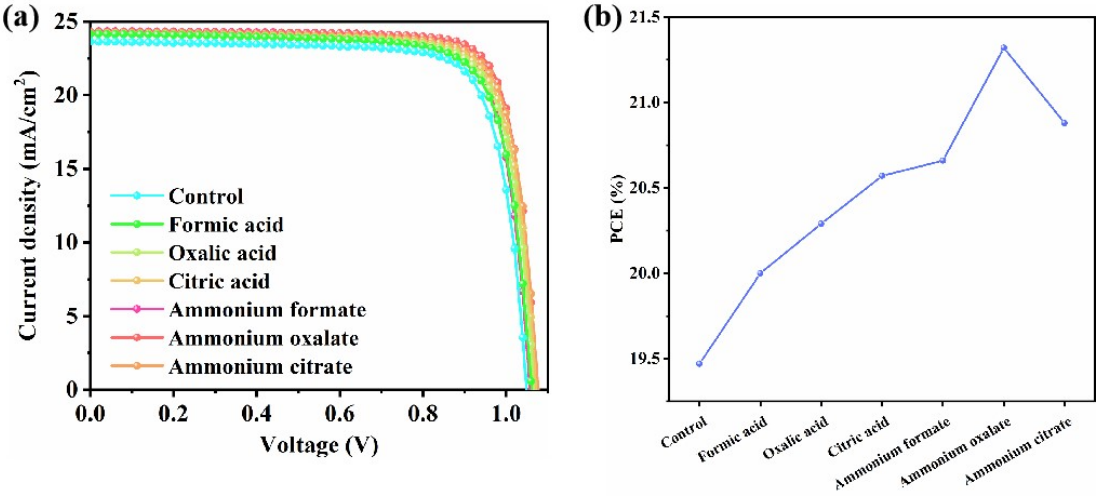

Figure S13. (a) Photovoltaic performance and J-V measurements of devices with different additive, and (b) efficiency comparison diagram.

Table S3. Specific photovoltaic parameters of the devices with different additive.

Samples	V_{oc} (V)	J_{sc} (mA/cm^2)	FF (%)	PCE (%)
Control	1.05	23.63	78.56	19.47
Formic acid	1.06	24.16	77.99	20.00
Oxalic acid	1.06	24.17	78.68	20.29
Citric acid	1.07	24.18	79.36	20.57
Ammonium formate	1.06	24.34	80.27	20.66
Ammonium oxalate	1.07	24.30	81.69	21.32
Ammonium citrate	1.07	24.23	79.98	20.88

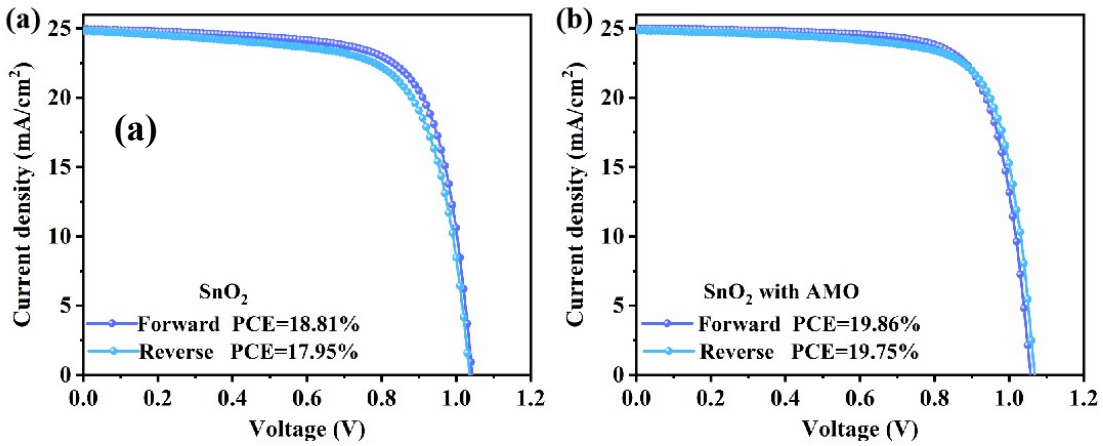

Figure S14. Photovoltaic performance and *J-V* measurements of (a) the control device and (b) the target device with a reverse scan (1.2 V ~-0.1 V, step: 0.01 V) and forward scan (-0.1 V ~1.2 V, step: 0.01 V), respectively.

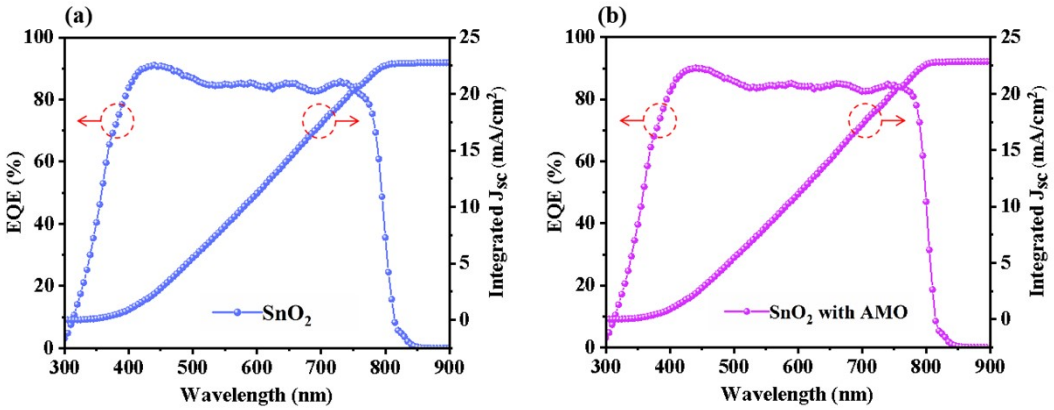

Figure S15. EQE spectra with the integrated J_{sc} of the control and target devices.

Table S4. Specific photovoltaic parameters of the devices before and after AMO modification under forward and reverse scanning.

Samples	V_{OC} (V)	J_{SC} (mA/cm^2)	FF (%)	PCE (%)
SnO_2-F	1.04	24.95	72.28	18.81
SnO_2-R	1.04	24.82	69.79	17.95
SnO_2 with AMO-F	1.06	25.03	75.03	19.86
SnO_2 with AMO-R	1.07	24.85	74.41	19.75

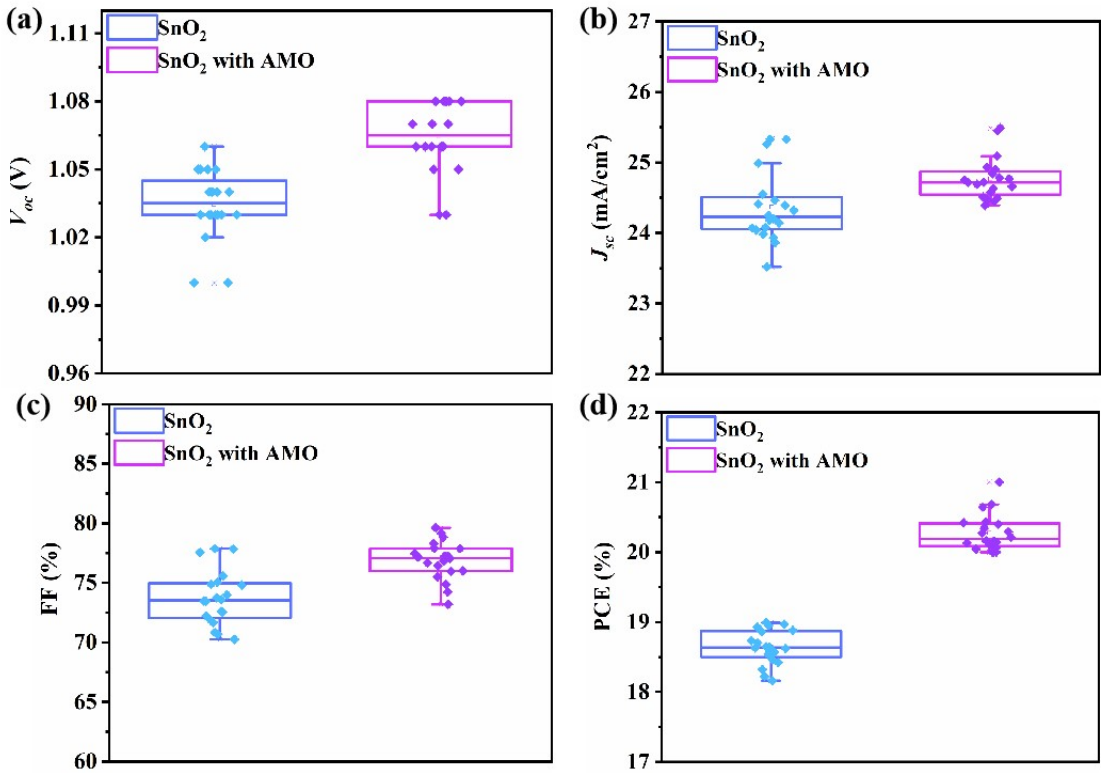

Figure S16. Photovoltaic performance variations for the control and target devices: (a) *V*oc, (b) *J*sc, (c) FF and (d) PCE of 20 devices.

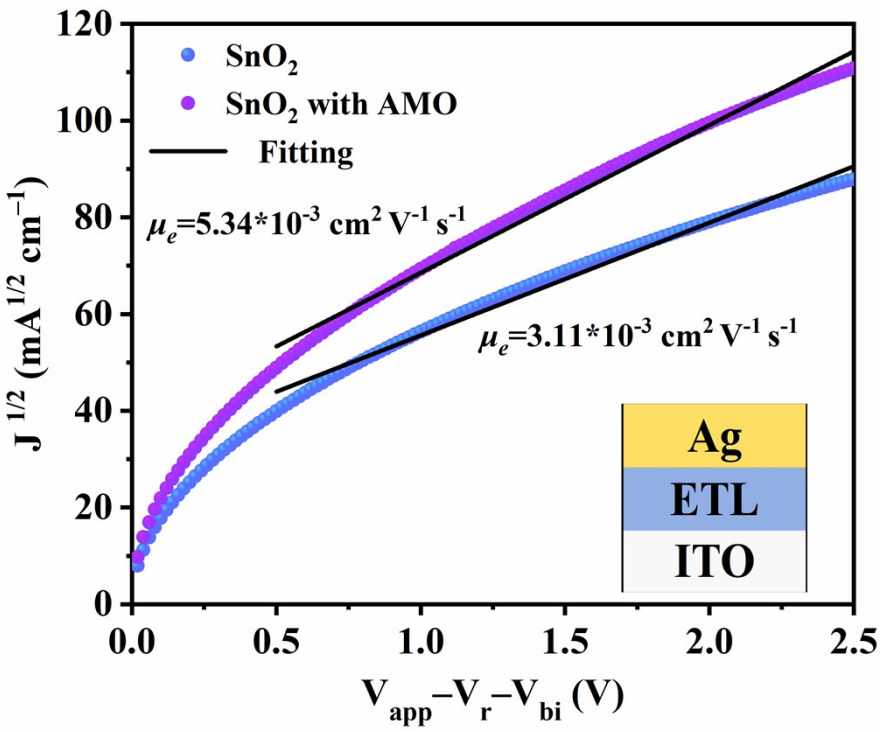

Figure S17. Electron mobility measurement of SnO_2 and SnO_2 with AMO by using the space-charge-limited current (SCLC) model with a device structure of ITO/ETL/Ag.

Table 3. EIS Parameters for the PSCs Based on the Pristine and Passivated SnO_2 ETLs.

Samples	R_s (Ω)	R_{rec} (Ω)
SnO_2	22.5	267.6
SnO_2 with AMO	19.4	448.6

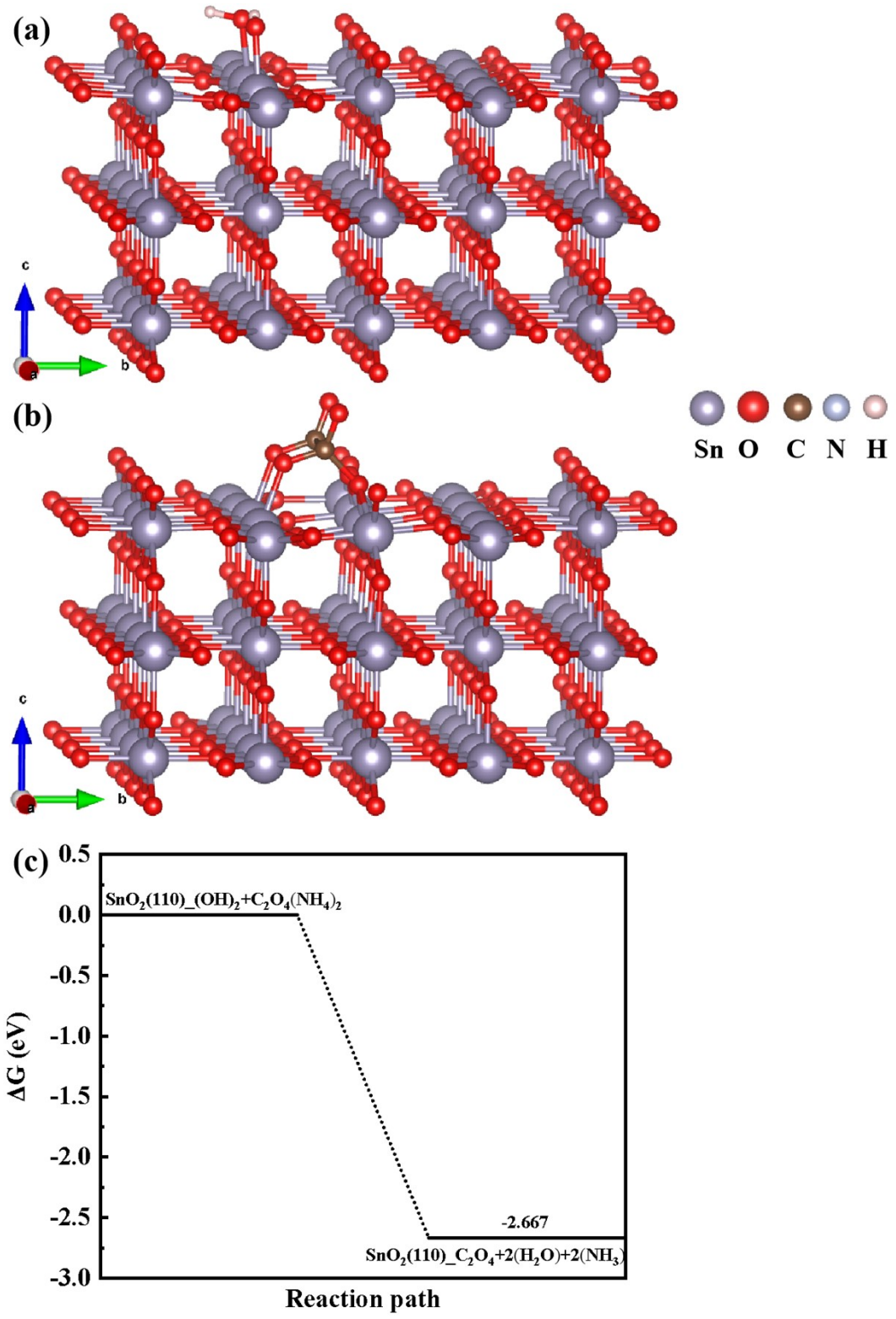

Figure S18. (a) $SnO_2(110)$ adsorption of $(OH)_2$ structure model; (b) $SnO_2(110)$ adsorption of C_2O_4 structure model; (c) the free energy of the reaction path.